Energy & Environmental Science

Flexible-Spacer Incorporated Polymer Donors Enable Superior Blend Miscibility for High-Performance and Mechanically-Robust Polymer Solar Cells

Journal:	*Energy & Environmental Science*
Manuscript ID	EE-ART-04-2021-001062.R1
Article Type:	Paper
Date Submitted by the Author:	07-May-2021
Complete List of Authors:	Lee, Jin-Woo ; Korea Advanced Institute of Science and Technology, Chemical and Biomolecular Engineering Jeong, Dahyun; Korea Advanced Institute of Science and Technology, Chemical and Biomolecular Engineering Kim, Dong Jun; Korea Advanced Institute of Science and Technology, Department of Mechanical Engineering Phan, Tan Ngoc-Lan; Korea Advanced Institute of Science and Technology, Chemical and Biomolecular Engineering Park, Jin Su; Korea Advanced Institute of Science and Technology, Chemical and Biomolecular Engineering Kim, Taek-Soo; Korea Advanced Institute of Science and Technology, Mechanical Engineering Kim, Bumjoon; Korea Advanced Institute of Science and Technology, Chemical and Biomolecular Engineering

Flexible-Spacer Incorporated Polymer Donors Enable Superior Blend Miscibility for High-Performance and Mechanically-Robust Polymer Solar Cells

Jin-Woo Lee,[†,a] *Dahyun Jeong,*[†,a] *Dong Jun Kim,*[b] *Tan Ngoc-Lan Phan,*[a] *Jin Su Park,*[a] *Taek-Soo Kim*[b] *and Bumjoon J. Kim*[*,a]

[a]Department of Chemical and Biomolecular Engineering, [b]Department of Mechanical Engineering, Korea Advanced Institute of Science and Technology (KAIST), Daejeon 34141, Republic of Korea

[*] All correspondence should be addressed to B. J. K. (E-mail: bumjoonkim@kaist.ac.kr)

KEYWORDS: polymer solar cell; polymer donor; non-fullerene small-molecule acceptor; mechanical robustness; high efficiency

Broader Context

Achieving sufficient mechanical reliability for highly efficient polymer solar cells (PSCs) is crucial for their potential application in various areas, where mechanical stress presents as a major cause for device failure. However, it is challenging to develop PSCs with both high power conversion efficiency (PCE) and mechanical robustness, as photoactive materials with planar and rigid backbones used for efficient PSCs result in brittle films with strong segregation. Here we develop an effective strategy to obtain highly efficient PSCs with remarkable mechanical robustness, by rational design of polymer donors (P_Ds) with aliphatic flexible spacer (FS) incorporated into a rigid polymer backbone. PSCs with PCEs of 17% and crack-onset strains (COSs) of 12% are demonstrated, which are among the most efficient and mechanically robust PSCs reported to date.

Abstract

Developing polymer solar cells (PSCs) with high photovoltaic performance and mechanical robustness is one of the most urgent tasks to ensure their operational reliability and applicability in wearable devices. However, it remains challenging to enhance the mechanical properties without compromising the electrical properties of high-performance active materials. Here, we develop a series of novel polymer donors (P_Ds), with which highly efficient PSCs having remarkable mechanical reliability are demonstrated. By interposing controlled amount of 1,10-di(thiophen-2-yl)decane flexible spacer (FS) into a PM6 backbone, we are able to significantly enhance the intermixing of the new P_Ds with small molecule acceptor (Y7), affording sufficient pathways for efficient charge percolation and mechanical stress dissipation. As a result, PSCs based on the P_D containing 5 mol% FS unit and Y7 exhibit a high power conversion efficiency (PCE) of 17% with a crack onset strain (COS) of 12% and a cohesive fracture energy (G_c) of 2.1 J m^{-2}, significantly outperforming the reference PM6-based devices (PCE = 15%, COS = 2% and G_c= 1.0 J m^{-2}). Both the photovoltaic performance and mechanical robustness of these PSCs are among the best values reported to date. The rational design of P_Ds demonstrated here presents a highly promising strategy to address the mechanical properties of SMA-based solar cells and their viable application in flexible/stretchable electronics.

Introduction

Development of reliable photovoltaic systems to harness sustainable energy resource is important in the face of energy crisis and environmental issue.[1-3] In particular, ensuring both high efficiency and mechanical robustness of polymer solar cells (PSCs) is an indispensable prerequisite for their operational stability and commercialization as power sources for next-generation wearable and portable devices.[3-5] Thanks to the recent development of benzodithiophene (BDT)-based polymer donors (P_Ds) and Y-series small molecule acceptors (SMAs), the power conversion efficiency (PCE) of PSCs has been significantly improved to around 17-18%.[6-12] However, the mechanical properties of these highly efficient PSCs are not sufficient to enable their practical application in flexible devices. For instance, most state-of-the-art P_D–SMA blends suffer from brittle mechanical properties with crack onset strains (COSs) of < 5%.[13-16] Therefore, there is an urgent need to enhance the mechanical robustness of PSCs while maintaining high PCEs.

To address this issue, the effects of molecular structure on the mechanical properties of P_D–SMA-based PSCs need to be carefully examined. To date, the molecular design of P_Ds for efficient PSCs has mainly followed a general approach of increasing the backbone planarity/rigidity to enhance the molecular interaction and charge transport ability,[17-20] which often result in strong phase segregation between P_D and SMA domains.[21-23] However, the large-size domains and weak donor–acceptor (D–A) interfaces caused by the high rigidity and low miscibility of active materials could also lead to numerous unconnected domains,[13,15,16,24] through which cracks are likely to propagate under mechanical stress.[13-15,25] Hence, to secure a sufficient amount of intermixed domains and favorable D–A interfaces in blend films, the backbone rigidity of P_Ds should be carefully modulated.[6,26] The intermixed phases here can also serve as percolation pathways between the domains to maintain high charge mobilities,

while suppressing the charge recombination of blend films.[27,28] Nevertheless, it is challenging to significantly reduce the backbone rigidity of P_Ds without compromising their electrical properties, as most efficient building blocks still comprise conjugated and fused structures.

Introducing flexible spacer (FS) units (*i.e.*, non-conjugated aliphatic chains) into a rigid P_D skeleton has been shown as an effective strategy for alleviating the P_D chain rigidity. Recently, various FS units have been employed to break polymer conjugation[29-31] and enhance the chain flexibility or mechanical ductility in the field of organic electronics (*i.e.*, organic field-effect transistors (OFETs)).[32-35] For example, Bao group inserted 2,6-pyridine dicarboxamide and alkyl segments into diketopyrrolopyrrole (DPP)-based polymers for use in OFETs with enhanced mechanical ductility, while retaining the electrical properties.[35,36] In addition, Thompson and Lipomi groups controlled lengths and contents of FS units in DPP-based polymers and demonstrated their relationships with mechanical/electrical properties.[33,34] However, the effects of FS units have been studied for the films based on pristine polymers and little has been explored for the blends, such as bulk-heterojunction (BHJ) blends. The mechanical and electrical properties of the blends are affected by morphological features, as well as material characteristics, owing to the presence of both intermixed and phase-separated domains of donor and acceptor materials.[37,38] Therefore, a systematic study is needed to elucidate the effects of FS units in P_D materials on both the electrical and mechanical properties, as well as their morphological behaviors in blends with acceptor materials.

In this work, we develop a series of P_Ds (PM6-CX, where X denotes the FS content = 5, 10, 20 and 30 mol%) by introducing 1,10-di(thiophen-2-yl)decane FS units into a poly[(2,6-(4,8-bis(5-(2-ethylhexyl-3-fluoro)thiophen-2-yl)-benzo[1,2-*b*:4,5-*b*′]dithiophene))-*alt*-(5,5-(1′,3′-di-2-thienyl-5′,7′-bis(2-ethylhexyl)benzo[1′,2′-*c*:4′,5′-*c*′]dithiophene-4,8-dione)] (PM6), with which both high photovoltaic performance and mechanical ductility are demonstrated.

Particularly, PCEs of ~17% are achieved for PSCs based on PM6-C5 and PM6-C10, in which small amounts (5 and 10 mol%) of the rigid benzodithiophenedione (BDD) units are replaced with the FS units, outperforming those of the reference PM6: 2,2'-((2*Z*,2'*Z*)-((12,13-bis(2-ethylhexyl)-3,9-diundecyl-12,13-dihydro-[1,2,5]thiadiazolo[3,4-e]thieno[2",3'':4',5']thieno[2',3':4,5]pyrrolo[3,2-g]thieno[2',3':4,5]thieno[3,2-b]indole-2,10-diyl)bis(methanylylidene))bis(5,6-dichloro-3-oxo-2,3-dihydro-1*H*-indene-2,1-diylidene))dimalononitrile (Y7) blends (PCE = 15%). Meanwhile, mechanical robustness is dramatically increased with a COS of 12%, a toughness of 3.67 MJ m^{-3}, and a cohesive fracture energy (G_c) of 2.1 J m^{-2} realized in the PM6-C5:Y7 blend, which are 6-, 14- and 2-fold higher than those of the PM6:Y7 blend, respectively. Detailed characterizations are performed to reveal how the structure of these new P_Ds affects the morphological, electrical and mechanical properties of P_D-SMA blends. It is found that improved intermixing between P_D and SMA in the blends is achieved upon the introduction of appropriate amounts of the FS unit, affording sufficient charge percolation and mechanical stress dissipation pathways. The best-performing blends containing PM6-C5 or PM6-C10 clearly exhibit suppressed growth of crystallites with lower domain purities as compared to the other blends, which are supported by differential scanning calorimetry (DSC) and resonant soft X-ray scattering (RSoXS) measurements.

Results and discussion

Synthesis and characterization of PM6-CX

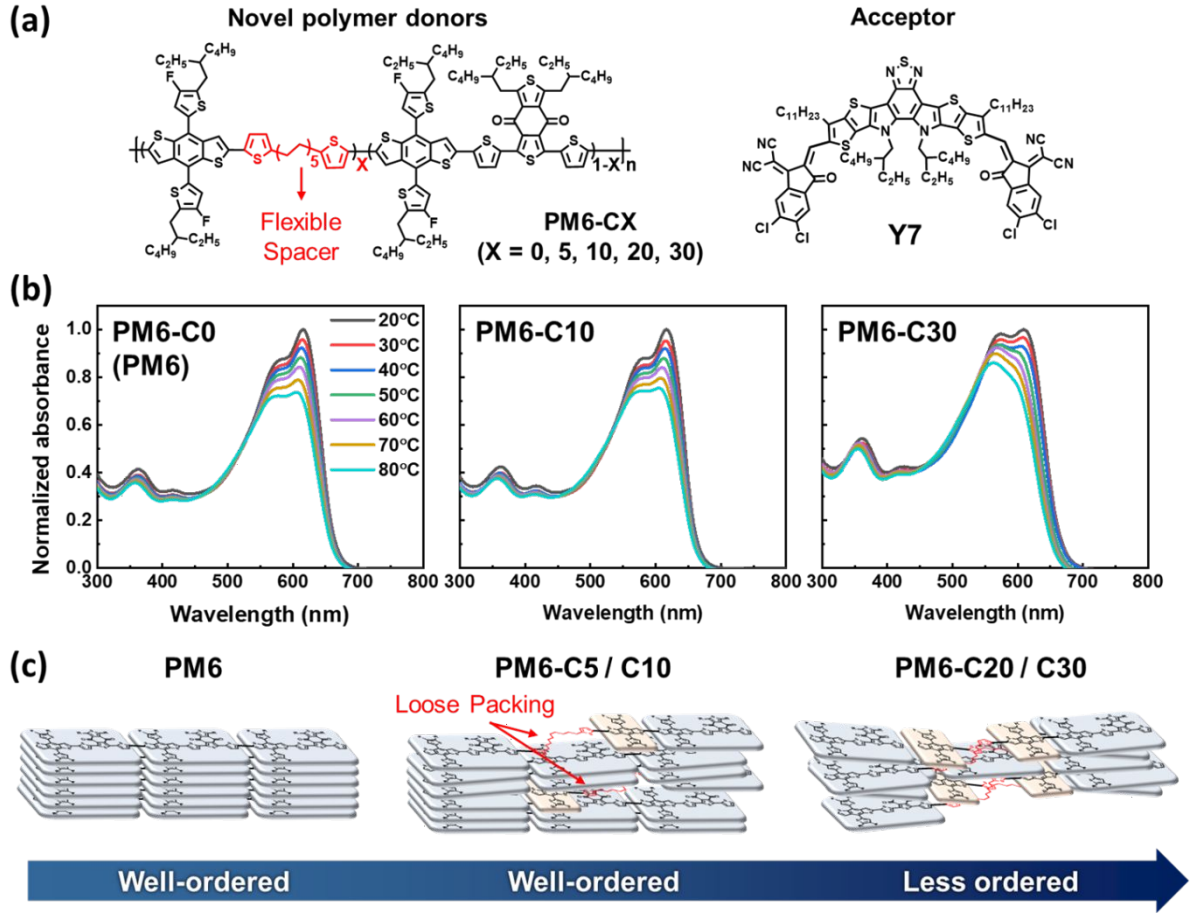

Fig. 1 (a) Chemical structures of P_Ds and SMA. (b) Temperature-dependent UV–Vis absorption spectra of P_Ds in CB solution. (c) Schematic illustrations for packing structures of P_Ds.

Table 1 Basic material properties of the PM6-CX P_Ds.

P_D	M_n ($Đ$) (kg mol^{-1})	λ_{max}^{film} (nm)[a]	$E_{g,opt}$ (eV)	μ_h (cm^2 V^{-1} s^{-1})[b]
PM6	27.3 (3.1)	619	1.82	4.2×10^{-4}
PM6-C5	29.1 (4.2)	619	1.85	3.1×10^{-4}
PM6-C10	29.1 (3.6)	619	1.85	3.2×10^{-4}
PM6-C20	31.7 (2.3)	609	1.86	9.4×10^{-5}
PM6-C30	28.3 (2.0)	610	1.84	5.9×10^{-5}

[a]Obtained from UV–Vis absorbance in the film state. [b]Calculated from SCLC mobility measurements.

The chemical structures of the P_Ds and SMA used in this study are shown in **Fig. 1**. We selected PM6-C0 (PM6), which offers fast charge transport and high light absorption, as the reference P_D.[39,40] A long FS building block was introduced as a third component to systematically decrease the backbone rigidity of the PM6 and optimize the blend morphology with SMA. The long decyl aliphatic chain was chosen to provide sufficient flexibility to the P_Ds, while not compromising the interchain interactions and electrical properties of the P_D.[41-43] A series of P_Ds were copolymerized by Stille coupling reactions,[44] varying the molar ratios of the BDD and FS units, while fixing the content of BDT. The resulting terpolymers were named PM6-CX (X = 0, 5, 10, 20 and 30), where X denotes the molar feed ratios of FS units compared with the total (FS + BDD) units. The nuclear magnetic resonance spectra of P_Ds, depending on the FS unit content, are shown in **Fig. S1**, **ESI**†. The molecular weights of the P_Ds were analyzed by high-temperature size-exclusion chromatography using 1,2,4-trichlorobenzene at 140 °C to prevent excessive pre-aggregation of the polymers during the measurement. All the P_Ds have number-average molecular weights (M_ns) within a similar range (27–31 kg mol^{-1}), minimizing the effects of molecular weight on their material properties (**Table 1**).[45] The molecular, optical and electrical characteristics of a series of PM6-CX P_Ds were investigated (**Table 1)**. The cyclic voltammograms and ultraviolet–visible (UV–Vis) absorption spectra in film states are shown in **Fig. S2**, **ESI**†. The PM6-C20 and PM6-C30 P_Ds exhibit slightly blue-shifted absorption with declined 0–0 transition peaks in the film state. These transitions are associated with the weaker aggregation of P_Ds resulting from the irregular backbone sequence with excessive FS units.[46,47]

To further investigate the effect of FS units on the aggregation properties of the P_Ds, temperature-dependent UV–Vis absorption spectra of the P_Ds in chlorobenzene solution were

monitored (**Fig. 1b** and **Fig. S3**, **ESI**†). The temperature-dependent aggregation (TDA) properties of P_Ds are considered crucial in controlling the blend morphology and achieving high photovoltaic performance, as the aggregated structures in solution highly impact the blend morphology in the film after solution processing.[48-50] The PM6-C5 and PM6-C10 P_Ds with small amounts of FS units showed TDA behaviors very similar to that of PM6. They showed almost the same maximum absorption wavelength (λ_{max}) values as PM6, and their 0–0 transition peaks were more prominent than the 0–1 transition peaks, even at elevated temperatures (**Fig. 1b**). Additionally, the hole mobilities (μ_hs), measured using a space-charge-limited current (SCLC) method, for PM6-C5 and PM6-C10 were comparable to that of PM6 (**Table 1**).[51] These results suggest that the appropriate interposition of the FS block did not compromise the aggregation and charge transport properties of the PM6-CX P_Ds (**Fig. 1c**).[48, 49] However, PM6-C20 and PM6-C30 showed significantly reduced 0–0 transition peaks and TDA properties in the solution UV–Vis absorption spectra. Additionally, the λ_{max} values of the absorption peaks were more blue-shifted compared with those of PM6. Consistently, the μ_hs of the PM6-C20 and PM6-C30 P_Ds were lower than that of the PM6 (**Table 1**). These results are mainly attributed to the presence of excessive FS units, which decrease the effective conjugation length and disturb the intrachain charge transfer in PM6-C20 and PM6-C30 (**Fig. 1c**).[32, 33, 52, 53]

Photovoltaic properties

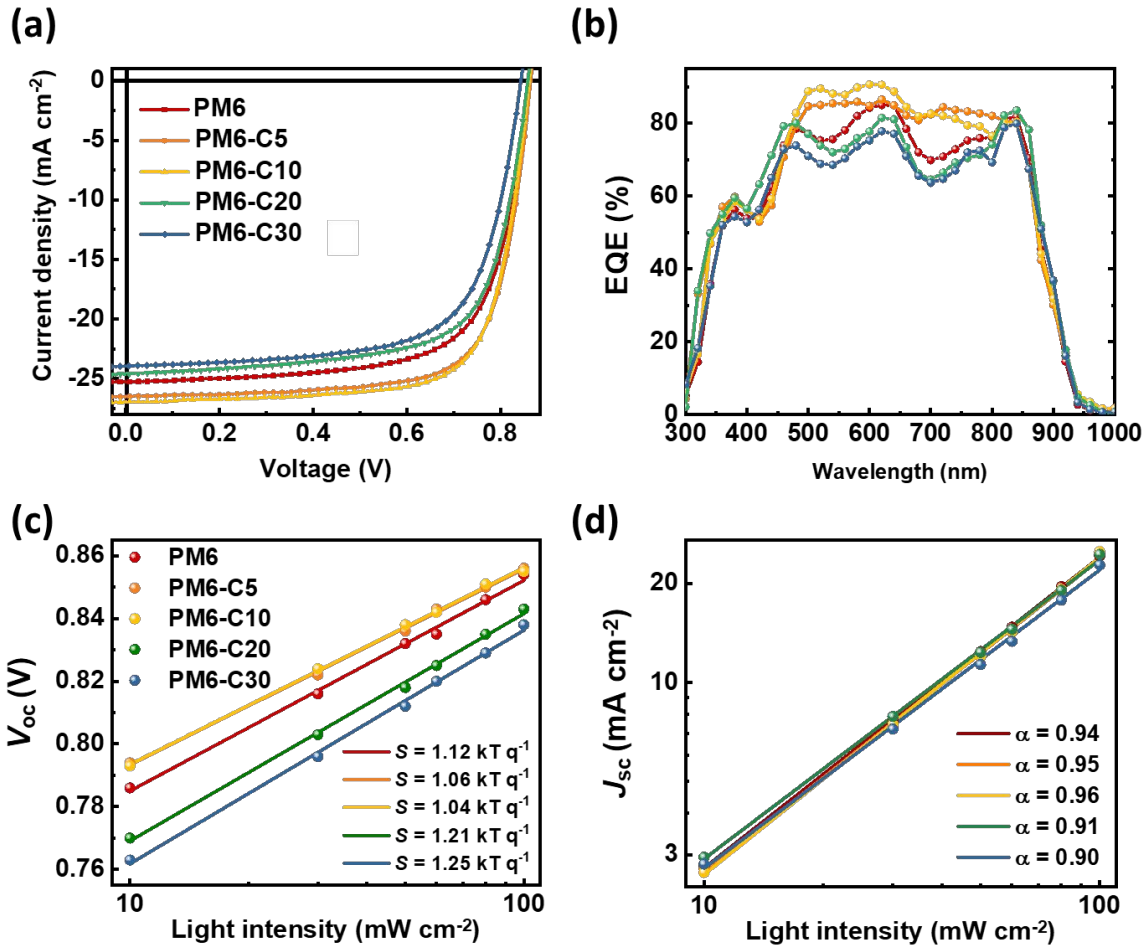

Fig. 2 (a) *J*–*V* curves; (b) EQE response spectra; dependences of (c) V_{oc} and (d) J_{sc} on light intensities of the PSCs.

Table 2 Photovoltaic performances of the PSCs depending on the P_D.

P_D	V_{oc} (V)[a]	J_{sc} (mA cm^{-2})[a]	Calc. J_{sc} (mA cm^{-2})	FF[a]	PCE$_{max\ (avg)}$ (%)[a]
PM6	0.86	25.4	25.0	0.69	15.1 (14.8)
PM6-C5	0.86	26.3	25.9	0.72	16.7 (16.2)
PM6-C10	0.86	26.8	26.2	0.74	17.0 (16.6)
PM6-C20	0.86	24.7	23.8	0.70	14.9 (14.7)
PM6-C30	0.84	23.9	23.1	0.68	13.8 (13.6)

[a]All parameters represent average values measured from more than ten PSC devices.

Next, we investigated the photovoltaic properties depending on the P_Ds by fabricating PSC devices with a normal-type device architecture. The *J*–*V* curves and corresponding photovoltaic parameters are presented in **Fig. 2a** and **Table 2**, respectively. The PM6:Y7-based PSC showed a high PCE of 15.1% with high J_{sc} (25.4 mA cm^{-2}) and FF (0.69) values. Interestingly, PCEs of the PM6-C5-and PM6-C10-based PSCs significantly increased to 16.7% and 17.0%, respectively. The main parameters that contributed to the increase in PCEs were J_{sc} and FF. For example, both the J_{sc} and FF values (J_{sc} = 25.4 mA cm^{-2} and FF = 0.69) of the PM6:Y7 blend increased to J_{sc} = 26.8 mA cm^{-2} and FF = 0.74 for the PM6-C10:Y7 blend. However, PCEs of the PM6-C20- and PM6-C30-based PSCs with P_Ds having excessive FS contents decreased to 14.9% and 13.8%, respectively. The external quantum efficiency (EQE) response spectra are shown in **Fig. 2b**. The calculated J_{sc} values agreed well with the ones obtained from the *J*-*V* curves within a 4% error range (**Table 2**). Compared with those of the other blends, the PM6-C5 and PM6-C10 blends showed higher EQE responses in the absorption ranges of both P_D (400 – 600 nm) and Y7 (700 – 900 nm). However, the PM6-C20 and PM6-C30 blends showed lower EQE responses throughout the absorption ranges. These results correspond well with the J_{sc} trends of PSC devices.

To understand the origin of the photovoltaic trends depending on the P_D, we examined the charge generation, transport and recombination properties of the P_D:Y7 blends. First, the charge generation properties of the blends were compared by calculating the exciton dissociation probabilities (*P*(E,T)s) from the photocurrent density (J_{ph}) versus effective voltage (V_{eff}) curves (**Fig. S4**, **ESI**†).[54] Although all the blends showed high *P*(E,T) values (over 93%), the PM6-C5:Y7 and PM6-C10:Y7 blends had even higher *P*(E,T) values (95%–96%). This suggests that, compared with the other blends, the PM6-C5:Y7 and PM6-C10:Y7 blends have better charge generation abilities at D–A interfaces. Subsequently, SCLC mobilities of the

blend films were measured to investigate their charge transport abilities (**Table S1**, **ESI**†). The μ_h values of the PM6-C5:Y7 and PM6-C10:Y7 blends were higher than that of the PM6:Y7 blend. However, both μ_h and electron mobility (μ_e) values of the PM6-C20:Y7 and PM6-C30:Y7 blends were significantly lower (*i.e.*, 1-order lower μ_h in magnitude) compared with those of the other blends, explaining their low J_{sc} values. Next, the dependences of J_{sc} and V_{oc} on light intensity (P) were examined to elucidate the charge recombination properties of the blends (**Fig. 2c** and **2d**). Generally, V_{oc} of PSCs is proportional to the natural logarithm of P, with the unit of kT q^{-1} (k = Boltzmann constant, T = temperature and q = elementary charge), and its slope (S) approaches unity when no monomolecular or trap-assisted recombination occurs before charge collection to electrodes.[55,56] It is known that J_{sc} values have a power-law relationship with P ($J_{sc} \propto P^{\alpha}$), and the α value reaches unity when bimolecular recombination does not occur in PSCs.[55] Notably, the PM6-C5:Y7 (S = 1.06 kT q^{-1}) and PM6-C10:Y7 (S = 1.04 kT q^{-1}) blends showed considerably suppressed monomolecular/trap-assisted recombinations compared with the PM6:Y7 blend (S = 1.12 kT q^{-1}) (**Fig. 2c**). However, the PM6-C20 (S = 1.21 kT q^{-1}) and PM6-C30 (S = 1.25 kT q^{-1}) blends showed deviated S values from unity. Additionally, the PM6-C20 and PM6-C30 blends showed highly deviated α values from unity (α = 0.90–0.91) in comparison with the other blends (α = 0.94–0.96), indicating that bimolecular recombination also occurs more strongly in these blends (**Fig. 2d**). Because charge recombination in PSCs affects their J_{sc} and FF,[55] the recombination properties support superior J_{sc} and FF values for the PM6-C5 and PM6-C10 blends compared with the other blends.

Morphological properties

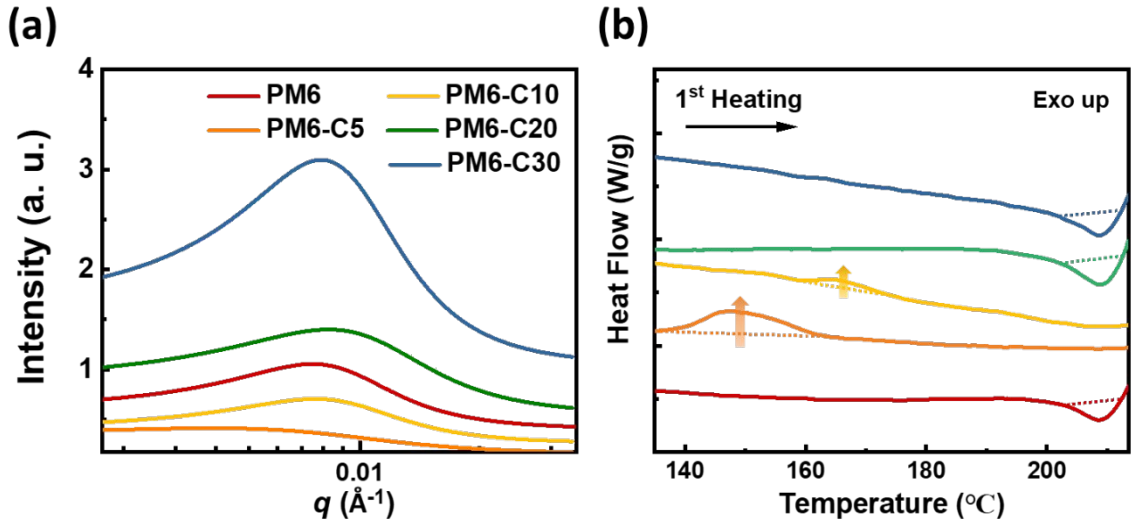

Fig. 3. (a) Lorentz-corrected RSoXS intensity profiles (measured beam energy: 284.4 eV); (b) DSC thermograms of the blend samples during the 1st heating cycle (dashed lines indicate the integrated ranges for ΔH_ms).

Table 3 Relative domain purities calculated from the RSoXS profiles and thermal properties of the P_D:Y7 blend and Y7 pristine samples during the 1st heating cycle of DSC measurement. The samples were prepared following the fabrication conditions in optimal PSC devices.

P_D	Relative domain purity[a]	T_{cc} (^{0}C)[b]	ΔH_{cc} (J g^{-1})[b]	T_m (^{0}C)[b]	ΔH_m (J g^{-1})[b]
PM6	0.52	–	–	208.8	0.36
PM6-C5	0.14	147.7	0.88	–	–
PM6-C10	0.24	166.0	0.19	–	–
PM6-C20	0.69	–	–	208.9	0.63
PM6-C30	1.00	–	–	208.5	0.38
Y7 Pristine	–	–	–	231.9	2.56

[a]Calculated from the RSoXS profiles. [b]Estimated from the DSC thermograms.

The enhanced photovoltaic and electrical properties of the PM6-C5- and PM6-C10-based PSCs can be attributed to their unique morphological properties. The morphological properties of all the blends were investigated by RSoXS, atomic force microscopy (AFM) and DSC measurements (**Fig. 3, S5** and **S6**, **ESI**†). The RSoXS profiles were obtained under a beam

energy of 284.4 eV, which can maximize the material contrast between P_Ds and SMA.[57] All the blends, except for the PM6-C5:Y7 blend, showed distinguishable peaks at approximately q = 0.008 Å^{-1} (domain spacing ~ 80 nm). However, the blends exhibited different peak intensities depending on the P_Ds. For more quantitative analysis, we estimated the relative domain purity of each blend, which is proportional to the square root of the integrated scattering intensity ($\sqrt{ISI}$) (**Table 3**).[58] Interestingly, a non-monotonic trend of the relative domain purities of the blends depending on the P_D was observed. The PM6-C5 and PM6-C10 blends showed considerably lower relative domain purities of 0.14 and 0.24, respectively, compared with that of the PM6:Y7 blend (0.52). However, the PM6-C20 and PM6-C30 blends exhibited higher values of 0.69 and 1.00, respectively, than the PM6 blend. This result indicates that introducing small portions of FS units into P_Ds (PM6-C5 and PM6-C10) significantly decreased the domain purities of the P_D and SMA domains while facilitating the generation of intermixed domains.[59] However, the excessive incorporation of FS units (PM6-C20 and PM6-C30) caused stronger phase separation between the P_D and SMA domains with high purities. A similar non-monotonic trend of the surface roughness of the PM6-CX:Y7 blends depending on the FS content was also observed in the AFM height images (**Fig. S5**, **ESI**†). The root-mean-square average roughness (R_q) was minimum at 1.0 nm for the PM6-C5:Y7 blend, while the other blends had higher R_q values. For example, the PM6-C30:Y7 blend had an R_q of 4.4 nm.

The DSC thermograms of the blends were compared, which showed very distinct thermal properties for the PM6-C5:Y7 and PM6-C10:Y7 blends (**Fig. 3b**). The samples were prepared following the fabrication condition of optimal PSC devices to elucidate the correlation between the morphological and photovoltaic properties of the devices. In detail, the blend films were prepared on glass substrates by the same film casting method (*i.e.*, spin coating) with device fabrication, and collected in DSC pans. Subsequently, the DSC curves during 1st heating cycles

were analyzed to directly investigate the morphological characteristic of the spin-coated blend films.[60] For the pristine P_Ds, there existed no recognizable endothermic and exothermic peaks, which are common phenomena for BDT-based P_Ds (**Fig. S6**, **ESI**†).[26] However, pristine Y7 showed a distinct melting transition peak at a melting temperature (T_m) of 231.9 °C, with a melting enthalpy (ΔH_m) of 2.56 J g^{-1} in the 1st heating cycle (**Fig. S6**, **ESI**† and **Table 3**). The high ΔH_m value was attributed to the strong intermolecular interactions from the highly rigid backbone of Y7 SMA.[61] The PM6:Y7, PM6-C20:Y7 and PM6-C30:Y7 blends also showed pronounced melting transition peaks with similar T_m values of approximately 209 °C and ΔH_ms in the range of 0.36–0.63 J g^{-1}, which belong to Y7 (**Fig. 3b** and **Table 3**). In contrast, the melting transition peaks completely disappeared in the cases of PM6-C5:Y7 and PM6-C10:Y7 blends. Instead, exothermic peaks appeared in the lower temperature range of 148–166 °C. These exothermic transitions in the heating cycle were attributed to the cold-crystallization process of Y7, often observed when imperfect crystals were developed in the blend film.[28,62,63] The PM6-C5 and PM6-C10 blends had cold-crystallization temperatures (T_{cc}s) of 148 and 166 °C, and cold-crystallization enthalpies (ΔH_{cc}s) of 0.88 J g^{-1} and 0.19 J g^{-1}, respectively. This result suggests that the formation of Y7 crystallites was significantly suppressed in the PM6-C5 and PM6-C10 blends compared with that in the PM6 blend.[63-65] And, the result is well supported by the UV–Vis absorption spectra of the blend films (**Fig. S7** and **Table S2**, **ESI**†). The PM6-C5- and PM6-C10-based blend films showed blue-shifted λ_{max} values (approximately 837 nm) of Y7 absorption, compared with the other blends showing λ_{max} in the range of 842–847 nm. This suggests that Y7 molecules were less aggregated/crystallized only in the PM6-C5 and PM6-C10 blends.[66]

To further understand the origin of different blend morphologies depending on the P_D, we analyzed the crystalline properties of the neat P_Ds by grazing-incidence X-ray scattering (GIXS)

measurements (**Fig. S8**, **ESI**†). Although the incorporation of the FS units gradually changed the orientation of the P_D packing structures from face-on to edge-on structure, the excessive growth of the P_D crystals in both the face-on and edge-on orientations was suppressed in the PM6-C5 and PM6-C10 films. Thus, the combined results from blend morphological analyses indicate that excessive crystal formation in both P_D and Y7 SMA was suppressed and, instead, more intermixed domains with larger P_D–SMA interfaces were developed in the PM6-C5:Y7 and PM6-C10:Y7 blends compared with the other blends.

Mechanical properties

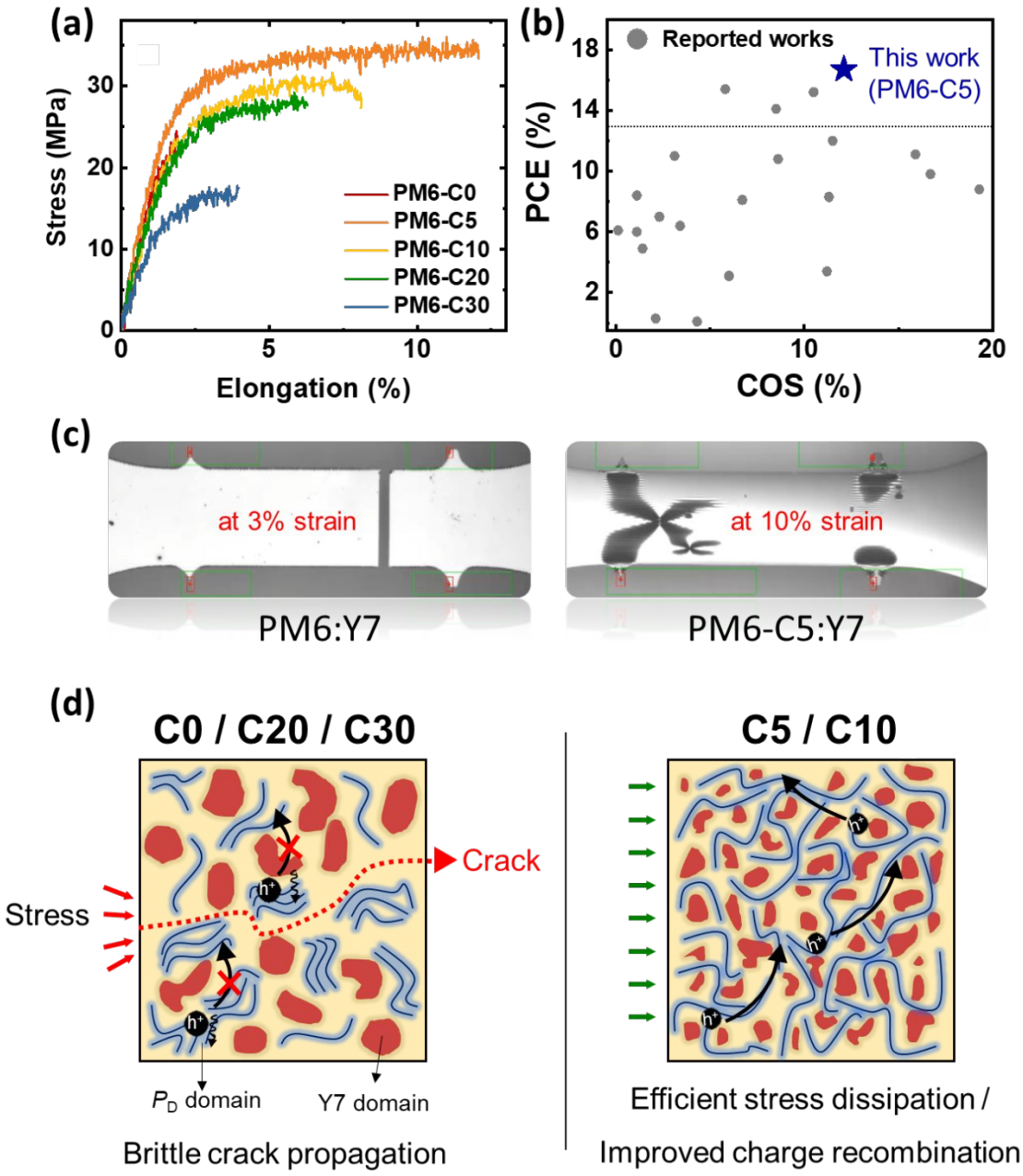

Fig. 5 (a) *S*–*S* curves for the P_D:Y7 blends, and (b) PCE versus COS curves for PSC blends from the reported works and this study (blend samples based on SMA or SMA-polymerized acceptor). (c) Images for the PM6:Y7 and PM6-C5:Y7 thin-films during the elongation are compared. The PM6:Y7 film is fractured at 3% strain, whereas wrinklings without any fracture are observed for the PM6-C5:Y7 film even at 10% strain. (d) Schematics illustrate different blend morphologies depending on the P_D.

Table 4 COS, toughness, elastic modulus and G_c values for the P_D:Y7 blends.

P_D	COS (%)[a]	Toughness (MJ m^{-3})[a]	E (GPa)[a]	G_c (J m^{-2})[b]
PM6	2.33 ± 0.12	0.26 ± 0.01	1.40 ± 0.03	1.01 ± 0.03
PM6-C5	12.09 ± 0.86	3.67 ± 0.14	1.54 ± 0.02	2.13 ± 0.40
PM6-C10	9.16 ± 1.24	2.03 ± 0.19	1.34 ± 0.02	1.62 ± 0.09
PM6-C20	6.19 ± 1.10	1.43 ± 0.38	1.17 ± 0.02	0.49 ± 0.01
PM6-C30	3.82 ± 1.04	0.50 ± 0.30	0.85 ± 0.02	0.49 ± 0.05

[a]The average values were calculated from more than three tensile samples. [b]Average values from three DCB samples.

The distinctive morphological properties of the PM6-C5:Y7 and PM6-C10:Y7 blends significantly impact their mechanical properties. First, the thin-film mechanical properties of the blends were investigated using the pseudo free-standing tensile test method (**Fig. 5** and **Table 4**). This method enables the measurement of the intrinsic tensile properties of thin films, excluding the effects of substrates.[67,68] The most interesting observation is the remarkably enhanced tensile properties of the PM6-C5:Y7 and PM6-C10:Y7 blends. The PM6:Y7 blend showed a brittle tensile behavior under mechanical strain, with a COS of only 2.33% and toughness of 0.26 MJ m^{-3}. However, the PM6-C5:Y7 blend had a COS of 12.09% and toughness of 3.67 MJ m^{-3}, which were 6 and 14 times higher than those for the PM6:Y7 blend, respectively. From the images obtained during elongation, it is evident that the PM6:Y7 blend showed sharp and brittle cracking at 3% strain, whereas the PM6-C5:Y7 blend underwent large plastic deformations with wrinkled features even at 10% strain (**Fig. 5c**). Interestingly, the excessive FS units in the P_Ds decreased both the COS and toughness values. For example, the COS and toughness of the PM6-C30:Y7 blend are 3.82% and 0.50 MJ m^{-3}, respectively. This indicates that the presence of large intermixed domains in the PM6-C5:Y7 and PM6-C10:Y7 blends had an impact on the tensile properties of the blend films.[69] The morphology in terms of domain purity and phase separation was optimized for the PM6-C5:Y7 blend, which

afforded PSCs with simultaneously enhanced PCE (17%) and COS (12%) values compared with the reference PM6:Y7 blend (PCE = 15% and COS = 2%). The PCE and COS values obtained in this study were compared with those of other studies (**Fig. 5b** and **Table S3**, **ESI**†).[13-16,70-74]

Next, the cohesion properties of the PSCs were evaluated by double cantilever beam (DCB) test methods. The sample structure and measured cohesive fracture energy (G_c) values are presented in **Table 4** and **Fig. S11**, **ESI**†. In addition, the load versus displacement curves are shown in **Fig. S12**, **ESI**†. After the test, it is confirmed that the fracture occurred within the active blend film. The PM6:Y7 blend showed a moderate G_c value of 1.01 J m^{-2}. In contrast, the blend samples with PM6-C5 (G_c = 2.13 J m^{-2}) and PM6-C10 (G_c = 1.62 J m^{-2}) P_Ds showed 2.1- and 1.6-fold higher G_c values than PM6:Y7 blend, respectively. The blends with PM6-C20 and PM6-C30 showed poor cohesion properties with G_c values of 0.49 J m^{-2}. The remarkably enhanced cohesion properties of the PM6-C5 and PM6-C10 blends could also be attributed to the presence of more developed intermixed domains than other blends, effectively dissipating mechanical stresses and enhancing adhesion/cohesion properties in the blends.[75-77]

To explore the potential of the enhanced mechanical properties of the PM6-C5- and PM6-C10-based blends, flexible PSC (FPSC) devices were fabricated and their photovoltaic properties investigated under continuous bending. The bending experiment and FPSCs are depicted in **Fig. S13**, **ESI**†. The *J–V* curves and normalized PCE values depending on the bending cycles are plotted in **Fig. S14**, **ESI**†. PM6-C5:Y7 blends showed a high initial PCE of 11.64% in the FPSC structure, outperforming that of PM6:Y7-based FPSC (PCE = 10.29%). Importantly, the PM6-C5:Y7-based FPSC exhibited better tolerance against the bending cycles compared with those of PM6:Y7-based FPSC (**Fig. S14**, **ESI**†). Thus, the use of PM6-C5 P_D enhanced both the photovoltaic and mechanical properties of the FPSC devices.

Schematic illustrations describe different morphologies and mechanical behaviors of the blends in **Fig. 5d**. The blends with P_Ds (PM6-C0, PM6-C20 and PM6-C30) without the FS unit or with excessive FS content underwent considerable phase separation between the P_D and SMA domains, resulting in higher domain purity. The isolated and pure domains make it difficult for free charges to hop into the other domains, inducing deteriorated charge mobilities and increased charge recombination in the blends. Furthermore, the weak adhesion/cohesion along the sharp interfaces between the P_D and SMA domains may provide a crack propagation pathway. In contrast, the PM6-C5:Y7 and PM6-C10:Y7 blends exhibited significantly improved blend morphologies with a larger portion of intermixed domains of P_D and SMA. These morphological features afford efficient charge generation and hopping through interconnected P_D and SMA networks. Importantly, the mechanical stresses in these blends can be effectively dissipated through the better-mixed domains.

Conclusion

In summary, we have developed a series of high-performance P_Ds by introducing various amounts of 1,10-di(thiophen-2-yl)decane FS units into a well-known rigid PM6 polymer backbone. It was found that a small content of FS units in PM6-C5 and PM6-C10 significantly improved the morphology of P_D–SMA blend, and restricted the overgrowth of P_D and SMA crystallites, without compromising any advantageous properties for efficient PSCs, such as pre-aggregation properties and hole mobilities. This led to the formation of favorable percolation pathways and the suppression of charge recombination. Owing to the augmented J_{sc} and *FF* compared with PM6, the best-performing P_Ds showed a superior PCE of 17%. Meanwhile, larger interfaces in the P_D–SMA blends enabled effective stress dissipation and unprecedented ductile behaviors of SMA-based binary blends. For instance, the PM6-C5-based blends afforded a superior COS of 12%, a toughness of 3.67 MJ m^{-3} and a G_c of 2.13 J m^{-2}, which are 6-, 14- and 2-fold increase as compared to those of PM6-based blends, respectively. Our work clearly shows that simultaneous enhancement of the photovoltaic performance and mechanical reliability can be achieved through the simple modification of molecular structures, moving PSCs a step closer to be used as power generators for flexible/stretchable electronics.

Experimental

General procedure for polymerization of PM6-CX: In a 20 mL vial, BDT monomer (100 μmol), BDD monomer (X μmol), 1,10-bis(5-bromothiophen-2-yl)decane [FS unit, (100-X) μmol] and $Pd(PPh_3)_4$ catalyst (3 μmol) were dissolved in 5 mL chlorobenzene and 0.5 mL *N*,*N*-dimethylformamide. Particularly, in the case of PM6-C20 and PM6-C30, toluene was used instead of chlorobenzene to elevate the molecular weights similar with those of the other P_Ds. The mole of added FS unit was decided to be X mol% of total dibromo-substituted (BDD + FS) units. After purging with argon, solution was stirred at the temperature of 120 °C for 36 h. The crude product was precipitated in methanol and purified through the Soxhlet extraction. The polymer was sequentially washed with methanol, acetone, hexane and THF, and extracted from chloroform. The final product was obtained after the precipitation of chloroform fraction in methanol and drying in vacuum oven.

Characterizations: UV-1800 spectrophotometer (Shimadzu Scientific Instruments) was used to obtain UV-Vis spectroscopy. Cyclic voltammograms were obtained from on an EG and G Parc model 273 Å system. DSC 25 (TA Instruments) was used to estimate thermal properties of the materials. RSoXS data were obtained in the Advanced Light Source (USA), 11.0.1.2 beamline. GIXS data were collected in Pohang Accelerator Laboratory (Republic of Korea), beamline 9A. L_c vales were estimated from the Scherrer equation:[78]

$$L_c = \frac{2\pi K}{\Delta_q}$$

K means shape factor (set to 0.9 in this work). Δ_q means full-with-half-maximum of each scattering.

Thin film tensile measurement: The tests were performed following the same sample structures and experimental procedures with the previously reported articles.[25, 79] A high-resolution load-cell was used to measure the load values under strains, and a constant strain rate (0.8×10^{-3} s^{-1}) was applied throughout the measurement. The results of more than three samples for each system were collected to obtain the average values and the standard deviations, which are presented in **Table 4**.

DCB test: The samples for the DCB test having a structure of glass/active layer/Au/epoxy (Epo-Tek 353ND, Epoxy Technology)/glass were fabricated by following the procedures in our previous report.[25] The results of more than three samples for each system were collected to obtain the average values and the standard deviations (**Table 4**). The critical strain energy release rates (G_cs) were estimated from the load cells having high resolution (Delaminator Adhesion Test System, DTS Company, Menlo Park, USA) in ambient conditions. The debond length (a) was obtained from following equations:[80]

$$G_c = \frac{12P_c^2a^2}{E'B^2h^3}\left(1 + \frac{0.64h}{a}\right)^2$$

$$a = \left(\frac{CE'Bh^3}{8}\right)^{\frac{1}{3}} - 0.64h$$

C = compliance ($d\delta/dP$), δ = displacement between beam ends and P_c = critical load, E' = plane strain modulus of the glass (= 76 GPa), B = width of specimen (= 8 mm) and h = half height of specimen.

Author contributions

J.-W.L. and D. J. equally contributed to conceptualization, analysis and writing the manuscript. D.J.K. and T.-S.K. carried out the analysis for mechanical properties. T.N.-L.P. and J.S.P. contributed to the characterization of the polymers and the device fabrication. B.J.K. supervised the entire process of the project.

Conflicts of interest

There are no conflicts to declare.

Acknowledgement

This work was supported by the National Research Foundation of Korea (NRF-2019R1A2B5B03101123 and 2020R1A4A1018516). The experiment at Advanced Light Source is supported by a DOE office of Science User Facility under contract no. DE-AC02-05CH11231. We acknowledge Seoyoung Kim and Changduk Yang (UNIST) for the help in SEC measurements.

References

1. L. Fagiolari, M. Bonomo, A. Cognetti, G. Meligrana, C. Gerbaldi, C. Barolo and F. Bella, *Chemsuschem*, 2020, **13**, 6562-6573.
2. N. Mariotti, M. Bonomo, L. Fagiolari, N. Barbero, C. Gerbaldi, F. Bella and C. Barolo, *Green Chemistry*, 2020, **22**, 7168-7218.
3. F. C. Krebs, T. D. Nielsen, J. Fyenbo, M. Wadstrom and M. S. Pedersen, *Energy Environ. Sci.*, 2010, **3**, 512-525.
4. C. Lee, S. Lee, G. U. Kim, W. Lee and B. J. Kim, *Chem. Rev.*, 2019, **119**, 8028-8086.
5. G. J. N. Wang, A. Gasperini and Z. A. Bao, *Adv. Electron. Mater.*, 2018, **4**, 1700429.
6. C. H. Cui and Y. F. Li, *Energy Environ. Sci.*, 2019, **12**, 3225-3246.
7. J. Q. Zhang, H. S. Tan, X. G. Guo, A. Facchetti and H. Yan, *Nat. Energy*, 2018, **3**, 720-731.
8. C. Li, H. T. Fu, T. Xia and Y. M. Sun, *Adv. Energy Mater.*, 2019, **9**, 1900999.
9. W. N. Li, L. Ye, S. S. Li, H. F. Yao, H. Ade and J. H. Hou, *Adv. Mater.*, 2018, **30**, 1707170.
10. W. Liu, X. Xu, J. Yuan, M. Leclerc, Y. P. Zou and Y. F. Li, *ACS Energy Lett.*, 2021, **6**, 598-608.
11. P. J. Chao, H. Chen, Y. L. Zhu, H. J. Lai, D. Z. Mo, N. Zheng, X. Y. Chang, H. Meng and F. He, *Adv. Mater.*, 2020, **32**, 1907059.
12. F. Lin, K. Jiang, W. Kaminsky, Z. L. Zhu and A. K. Y. Jen, *J. Am. Chem. Soc.*, 2020, **142**, 15246-15251.
13. J.-W. Lee, C. Sun, B. S. Ma, H. J. Kim, C. Wang, J. M. Ryu, C. Lim, T. S. Kim, Y. H. Kim, S. K. Kwon and B. J. Kim, *Adv. Energy Mater.*, 2021, **11**, 2003367.
14. Q. P. Fan, W. Y. Su, S. S. Chen, W. Kim, X. B. Chen, B. Lee, T. Liu, U. A. Mendez-Romero, R. J. Ma, T. Yang, W. L. Zhuang, Y. Li, Y. W. Li, T. S. Kim, L. T. Hou, C. Yang, H. Yan, D. H. Yu and E. G. Wang, *Joule*, 2020, **4**, 658-672.
15. J. Choi, W. Kim, S. Kim, T. S. Kim and B. J. Kim, *Chem. Mater.*, 2019, **31**, 9057-9069.
16. T. Kim, J. H. Kim, T. E. Kang, C. Lee, H. Kang, M. Shin, C. Wang, B. W. Ma, U. Jeong, T. S. Kim and B. J. Kim, *Nat. Commun.*, 2015, **6**, 8547.
17. W. C. Zhao, S. S. Li, H. F. Yao, S. Q. Zhang, Y. Zhang, B. Yang and J. H. Hou, *J. Am. Chem. Soc.*, 2017, **139**, 7148-7151.
18. H. T. Fu, Z. H. Wang and Y. M. Sun, *Angew. Chem. Int. Ed.*, 2019, **58**, 4442-4453.
19. J. H. Chen, L. Wang, J. Yang, K. Yang, M. A. Uddin, Y. M. Tang, X. Zhou, Q. G. Liao, J. W. Yu, B. Liu, H. Y. Woo and X. G. Guo, *Macromolecules*, 2019, **52**, 341-353.
20. N. Wang, S. Zhang, R. Y. Zhao, J. R. Feng, Z. C. Ding, W. Ma, J. L. Hu and J. Liu, *ACS Appl. Electron. Mater.*, 2020, **2**, 2274-2281.
21. X. Guo, Q. P. Fan, J. N. Wu, G. W. Li, Z. X. Peng, W. Y. Su, J. Lin, L. T. Hou, Y. P. Qin, H. Ade, L. Ye, M. J. Zhang and Y. F. Li, *Angew. Chem. Int. Ed.*, 2021, **60**, 2322-2329.
22. Z. H. Liao, K. Yang, L. C. Hou, J. Li, J. Lv, R. Singh, M. Kumar, Q. Q. Chen, X. Y. Dong, T. L. Xu, C. Hu, T. N. Duan, Z. P. Kan, S. R. Lu and Z. Y. Xiao, *Macromolecules*, 2020, **53**, 9034-9042.
23. J. N. Wu, G. W. Li, J. Fang, X. Guo, L. Zhu, B. Guo, Y. L. Wang, G. Y. Zhang, L. Arunagiri, F. Liu, H. Yan, M. J. Zhang and Y. F. Li, *Nat. Commun.*, 2020, **11**, 4612.

24. K. Feng, Z. Wu, M. Y. Su, S. X. Ma, Y. Q. Shi, K. Yang, Y. Wang, Y. J. Zhang, W. P. Sun, X. Cheng, L. M. Huang, J. Min, H. Y. Woo and X. G. Guo, *Adv. Funct. Mater.*, 2021, **31**, 2008494.

25. J.-W. Lee, B. S. Ma, J. Choi, J. Lee, S. Lee, K. Liao, W. Lee, T. S. Kim and B. J. Kim, *Chem. Mater.*, 2020, **32**, 582-594.

26. Z. Zheng, H. F. Yao, L. Ye, Y. Xu, S. Q. Zhang and J. H. Hou, *Mater. Today*, 2020, **35**, 115-130.

27. J. W. Lee, M. J. Sung, D. Kim, S. Lee, H. You, F. S. Kim, Y. H. Kim, B. J. Kim and S. K. Kwon, *Chem. Mater.*, 2020, **32**, 2572-2582.

28. M. Ghasemi, H. W. Hu, Z. X. Peng, J. J. Rech, I. Angunawela, J. H. Carpenter, S. J. Stuard, A. Wadsworth, I. McCulloch, W. You and H. Ade, *Joule*, 2019, **3**, 1328-1348.

29. A. X. Chen, A. T. Kleinschmidt, K. Choudhary and D. J. Lipomi, *Chem. Mater.*, 2020, **32**, 7582-7601.

30. X. K. Zhao, Y. Zhao, Q. Ge, K. Butrouna, Y. Diao, K. R. Graham and J. G. Mei, *Macromolecules*, 2016, **49**, 2601-2608.

31. A. Gasperini, S. Bivaud and K. Sivula, *Chem. Sci.*, 2014, **5**, 4922-4927.

32. L. A. Galuska, W. W. McNutt, Z. Y. Qian, S. Zhang, D. W. Weller, S. Dhakal, E. R. King, S. E. Morgan, J. D. Azoulay, J. G. Mei and X. D. Gu, *Macromolecules*, 2020, **53**, 6032-6042.

33. E. L. Melenbrink, K. M. Hilby, K. Choudhary, S. Samal, N. Kazerouni, J. L. McConn, D. J. Lipomi and B. C. Thompson, *ACS Appl. Polym. Mater.*, 2019, **1**, 1107-1117.

34. E. L. Melenbrink, K. M. Hilby, M. A. Alkhadra, S. Samal, D. J. Lipomi and B. C. Thompson, *ACS Appl. Mater. Interfaces*, 2018, **10**, 32426-32434.

35. J. Y. Oh, S. Rondeau-Gagne, Y. C. Chiu, A. Chortos, F. Lissel, G. J. N. Wang, B. C. Schroeder, T. Kurosawa, J. Lopez, T. Katsumata, J. Xu, C. X. Zhu, X. D. Gu, W. G. Bae, Y. Kim, L. H. Jin, J. W. Chung, J. B. H. Tok and Z. N. Bao, *Nature*, 2016, **539**, 411-415.

36. J. W. Mun, G. J. N. Wang, J. Y. Oh, T. Katsumata, F. L. Lee, J. Kang, H. C. Wu, F. Lissel, S. Rondeau-Gagne, J. B. H. Tok and Z. A. Bao, *Adv. Funct. Mater.*, 2018, **28**, 1804222.

37. S. Savagatrup, D. Rodriquez, A. D. Printz, A. B. Sieval, J. C. Hummelen and D. J. Lipomi, *Chem. Mater.*, 2015, **27**, 3902-3911.

38. J.-W. Lee, N. Choi, D. Kim, T. N.-L. Phan, H. Kang, T.-S. Kim and B. J. Kim, *Chem. Mater.*, 2021, **33**, 1070-1081.

39. M. J. Zhang, X. Guo, W. Ma, H. Ade and J. H. Hou, *Adv. Mater.*, 2015, **27**, 4655-4660.

40. Y. Cui, H. F. Yao, J. Q. Zhang, T. Zhang, Y. M. Wang, L. Hong, K. H. Xian, B. W. Xu, S. Q. Zhang, J. Peng, Z. X. Wei, F. Gao and J. H. Hou, *Nat. Commun.*, 2019, **10**, 2515.

41. L. Ding, H. B. Li, T. Lei, H. Z. Ying, R. B. Wang, Y. Zhou, Z. M. Su and J. Pei, *Chem. Mater.*, 2012, **24**, 1944-1949.

42. A. Rahmanudin, L. Yao and K. Sivula, *Polym. J.*, 2018, **50**, 725-736.

43. G. Grasso and J. J. Titman, *Macromolecules*, 2009, **42**, 4175-4180.

44. B. Carsten, F. He, H. J. Son, T. Xu and L. P. Yu, *Chem. Rev.*, 2011, **111**, 1493-1528.

45. M. M. Shi, T. Wang, Y. Wu, R. Sun, W. Wang, J. Guo, Q. Wu, W. Y. Yang and J. Min, *Adv. Energy Mater.*, 2021, **11**, 2002709.

46. T. Erdmann, S. Fabiano, B. Milian-Medina, D. Hanifi, Z. H. Chen, M. Berggren, J. Gierschner, A. Salleo, A. Kiriy, B. Voit and A. Facchetti, *Adv. Mater.*, 2016, **28**, 9169-9174.

47. B. C. Schroeder, Y. C. Chiu, X. D. Gu, Y. Zhou, J. Xu, J. Lopez, C. Lu, M. F. Toney and Z. N. Bao, *Adv. Electron. Mater.*, 2016, **2**, 1600104.

48. H. W. Hu, P. C. Y. Chow, G. Y. Zhang, T. X. Ma, J. Liu, G. F. Yang and H. Yan, *Acc. Chem. Res.*, 2017, **50**, 2519-2528.

49. S. Seo, J. Kim, H. Kang, J.-W. Lee, S. Lee, G. U. Kim and B. J. Kim, *Macromolecules*, 2021, **54**, 53-63.

50. N. Wang, Y. J. Yu, R. Y. Zhao, Z. C. Ding, J. Liu and L. X. Wang, *Macromolecules*, 2020, **53**, 3325-3331.

51. Z. Chiguvare and V. Dyakonov, *Phys. Rev. B*, 2004, **70**, 235207.

52. S. Savagatrup, X. K. Zhao, E. Chan, J. G. Mei and D. J. Lipomi, *Macromol. Rapid Commun.*, 2016, **37**, 1623-1628.

53. Y. Zhao, X. K. Zhao, Y. P. Zang, C. A. Di, Y. Diao and J. G. Mei, *Macromolecules*, 2015, **48**, 2048-2053.

54. P. W. M. Blom, V. D. Mihailetchi, L. J. A. Koster and D. E. Markov, *Adv. Mater.*, 2007, **19**, 1551-1566.

55. S. R. Cowan, A. Roy and A. J. Heeger, *Phys. Rev. B*, 2010, **82**, 245207.

56. L. J. A. Koster, M. Kemerink, M. M. Wienk, K. Maturova and R. A. J. Janssen, *Adv. Mater.*, 2011, **23**, 1670-1674.

57. C. Lee, T. Giridhar, J. Choi, S. Kim, Y. Kim, T. Kim, W. Lee, H. H. Cho, C. Wang, H. Ade and B. J. Kim, *Chem. Mater.*, 2017, **29**, 9407-9415.

58. H. W. Hu, Y. K. Li, J. Q. Zhang, Z. X. Peng, L. K. Ma, J. M. Xin, J. C. Huang, T. X. Ma, K. Jiang, G. Y. Zhang, W. Ma, H. Ade and H. Yan, *Adv. Energy Mater.*, 2018, **8**, 1800234.

59. S. Mukherjee, C. M. Proctor, G. C. Bazan, T. Q. Nguyen and H. Ade, *Adv. Energy Mater.*, 2015, **5**, 1500877.

60. D. Baran, R. S. Ashraf, D. A. Hanifi, M. Abdelsamie, N. Gasparini, J. A. Röhr, S. Holliday, A. Wadsworth, S. Lockett, M. Neophytou, C. J. M. Emmott, J. Nelson, C. J. Brabec, A. Amassian, A. Salleo, T. Kirchartz, J. R. Durrant and I. McCulloch, *Nat. Mater.*, 2017, **16**, 363-369.

61. M. Zhang, L. Zhu, T. Y. Hao, G. Q. Zhou, C. Q. Qiu, Z. Zhao, N. Hartmann, B. Xiao, Y. C. Zou, W. Feng, H. M. Zhu, M. J. Zhang, Y. M. Zhang, Y. F. Li, T. P. Russell and F. Liu, *Adv. Mater.*, 2021, 2007177.

62. M. Ghasemi, N. Balar, Z. X. Peng, H. W. Hu, Y. P. Qin, T. Kim, J. J. Rech, M. Bidwell, W. Mask, I. McCulloch, W. You, A. Amassian, C. Risko, B. T. O'Connor and H. Ade, *Nat. Mater.*, 2021, **20**, 525–532.

63. J. M. Xin, X. Y. Meng, X. B. Xu, Q. L. Zhu, H. B. Naveed and W. Ma, *Matter*, 2019, **1**, 1316-1330.

64. B. J. Lin, X. B. Zhou, H. Zhao, J. Yuan, K. Zhou, K. Chen, H. B. Wu, R. J. Guo, M. A. Scheel, A. Chumakov, S. V. Roth, Y. M. Mao, L. L. Wang, Z. Tang, P. Muller-Buschbaum and W. Ma, *Energy Environ. Sci.*, 2020, **13**, 2467-2479.

65. C. H. Zhang, A. Mumyatov, S. Langner, J. D. Perea, T. Kassar, J. Min, L. L. Ke, H. W. Chen, K. L. Gerasimov, D. V. Anokhin, D. A. Ivanov, T. Ameri, A. Osvet, D. K. Susarova, T. Unruh, N. Li, P. Troshin and C. J. Brabec, *Adv. Energy Mater.*, 2017, **7**, 1601204.

66. B. B. Qiu, Z. Chen, S. C. Qin, J. Yao, W. C. Huang, L. Meng, H. M. Zhu, Y. Yang, Z. G. Zhang and Y. F. Li, *Adv. Mater.*, 2020, **32**, 1908373.

67. J. H. Kim, A. Nizami, Y. Hwangbo, B. Jang, H. J. Lee, C. S. Woo, S. Hyun and T. S. Kim, *Nat. Commun.*, 2013, **4**, 2520.

68. J.-W. Lee, B. S. Ma, H. J. Kim, T.-S. Kim and B. J. Kim, *JACS Au*, 2021, DOI: 10.1021/jacsau.1c00064.

69. B. J. Lin, L. Zhang, H. Zhao, X. B. Xu, K. Zhou, S. Zhang, L. Gou, B. B. Fan, L. Zhang, H. P. Yan, X. D. Gu, L. Ying, F. Huang, Y. Cao and W. Ma, *Nano Energy*, 2019, **59**, 277-284.

70. J. H. Kim, J. Noh, H. Choi, J. Y. Lee and T. S. Kim, *Chem. Mater.*, 2017, **29**, 3954-3961.

71. Y. L. Wang, Q. L. Zhu, H. B. Naveed, H. Zhao, K. Zhou and W. Ma, *Adv. Energy Mater.*, 2020, **10**, 1903609.

72. J. H. Han, F. Bao, D. Huang, X. C. Wang, C. M. Yang, R. Q. Yang, X. G. Jian, J. Y. Wang, X. C. Bao and J. H. Chu, *Adv. Funct. Mater.*, 2020, **30**, 2003654.

73. W. Lee, J. H. Kim, T. Kim, S. Kim, C. Lee, J. S. Kim, H. Ahn, T. S. Kim and B. J. Kim, *J. Mater. Chem. A*, 2018, **6**, 4494-4503.

74. Q. Wu, W. Wang, Y. Wu, Z. Chen, J. Guo, R. Sun, J. Guo, Y. Yang and J. Min, *Adv. Funct. Mater.*, 2021, **31**, 2010411.

75. C. Bruner, F. Novoa, S. Dupont and R. Dauskardt, *ACS Appl. Mater. Interfaces*, 2014, **6**, 21474-21483.

76. C. Bruner, N. C. Miller, M. D. McGehee and R. H. Dauskardt, *Adv. Funct. Mater.*, 2013, **23**, 2863-2871.

77. N. Balar, Y. Xiong, L. Ye, S. S. Li, D. Nevola, D. B. Dougherty, J. H. Hou, H. Ade and B. T. O'Connor, *ACS Appl. Mater. Interfaces*, 2017, **9**, 43886-43892.

78. J. Rivnay, S. C. B. Mannsfeld, C. E. Miller, A. Salleo and M. F. Toney, *Chem. Rev.*, 2012, **112**, 5488-5519.

79. J. Choi, W. Kim, D. Kim, S. Kim, J. Chae, S. Q. Choi, F. S. Kim, T. S. Kim and B. J. Kim, *Chem. Mater.*, 2019, **31**, 3163-3173.

80. M. F. Kanninen, *Int. J. Frac.*, 1973, **9**, 83-92.